MICROBOONE-NOTE-1133-PUB
September 16, 2024

# First measurement of differential cross sections for muon neutrino charged current interactions on argon with a two-proton final state using the MicroBooNE detector

The MicroBooNE Collaboration

**Abstract**

We present the first measurement of differential cross sections for charged-current muon neutrino interactions on argon with one muon, two protons, and no pions in the final state. These final states are dominated by two-nucleon knockout interactions, which are complicated to model and there is currently limited information about the characteristics of these interactions in existing neutrino-nucleus scattering data. Detailed investigations of two-nucleon knockout are vital to support upcoming experiments exploring the nature of the neutrino. Among the different kinematic quantities measured, the opening angle between the two protons, the angle between the total proton momentum and the muon, and the total transverse momentum of the final state system are most sensitive to the underlying physics processes as embodied in various theoretical models.

*Keywords:* neutrinos, argon, cross section, charged-current interactions, 2-particle 2-hole states

## 1. Introduction

The introduction of the liquid argon time projection chamber (LArTPC) [1, 2, 3, 4] has revolutionized the field of accelerator-based neutrino physics, allowing a more detailed observation of ionizing radiation in the final state than was previously possible. This development, in turn, has highlighted the need for advanced modeling of neutrino-nucleus interactions, especially neutrino-argon interactions, and detailed measurements to benchmark those models. Cross-section measurements of a variety of different final state topologies for an array of different nuclei are needed to support the development of neutrino interaction models [5]. These models must address both in-medium nuclear modification of the fundamental neutrino interactions and also final-state interactions (FSI) involving the reaction products as they exit the nucleus [6].

One process that probes both neutrino interactions and nuclear effects is the production of two-particle two-hole (2p2h) states in which two nucleons are removed from the nucleus. These

*Email address:* microboone_info@fnal.gov (The MicroBooNE Collaboration)

states are primarily produced by neutrino interactions where the momentum transfer is shared between two nucleons via the exchange of a virtual meson, known as a meson exchange current (MEC) [6]. In addition, 2p2h states can be produced by nuclear effects, such as short-range nucleon-nucleon correlations (SRC) [7, 8] and FSI. In the case of SRCs, the neutrino interacts with a nucleon that is part of a correlated nucleon-nucleon pair. The momentum is transferred to a single nucleon but, because this nucleon is part of a correlated pair, both nucleons are knocked out of the nucleus. In the case of FSI, it is possible for a single nucleon to knock out a second nucleon as it exits the nucleus thereby leading to a 2p2h final state. Observation of 2p2h states in electron scattering has been used to develop the models [9] of 2p2h production in neutrino scattering and the implementation [10] thereof. Correct modeling of 2p2h interactions is of vital importance to neutrino energy reconstruction and precision measurements of neutrino oscillations, but their production cross section has never been measured directly in neutrino scattering.

A final state topology consistent with the production of a 2p2h state is a charged-current (CC) muon neutrino ($\nu_\mu$) interaction that results in one muon, two protons, and no charged or neutral pions (CC1$\mu$2p0$\pi$). While there is an existing measurement of CC1$\mu$2p0$\pi$ events on argon, no cross sections were extracted [11]. In this letter, we present the first differential cross section measurements of CC1$\mu$2p0$\pi$ topologies on argon using data collected from the Micro Booster Neutrino Experiment (MicroBooNE) [12].

## 2. Detector and Samples

The MicroBooNE experiment uses an 85 metric ton fiducial volume LArTPC detector located at Fermi National Accelerator Laboratory [12]. The detector is situated on-axis to the Booster Neutrino Beam (BNB) which has an average energy of $\langle E_\nu \rangle = 0.8$ GeV [13] and is located approximately 470 m from the neutrino production target. The detector consists of two components: a TPC, 10.36 m long in the beam direction, 2.56 m wide in the drift direction, and 2.32 m tall; and an optical system comprised of 32 eight-inch photomultiplier tubes (PMTs). The TPC consists of three wire planes, two induction planes and one collection plane. The collection plane is oriented vertically and the induction plane wires are oriented at angles $\pm 60^\circ$ with respect to the vertical direction. Electronic signals from the TPC wire planes and the PMTs are recorded and subdivided into two distinct data samples. The first sample, known as on-beam data (BNB data), is collected coincident to a $1.6\,\mu s$ BNB neutrino spill. The second sample, known as off-beam data (EXT data), is recorded outside of the BNB spill. This sample provides a measure of the electronic noise and large cosmic muon background caused by the surface location of the MicroBooNE detector. The BNB data and a portion of the EXT data samples are then filtered based on a required minimum amount of activity measured in the PMTs. This study uses data from the three-year period 2016-2018, corresponding to $6.85 \times 10^{20}$ protons on target.

MicroBooNE utilizes the GENIE neutrino event generator [14] to create two samples of simulated neutrino interactions: (1) overlay Monte Carlo (overlay MC) which addresses signal events and beam-related backgrounds, (2) dirt Monte Carlo (dirt MC) which addresses backgrounds from neutrino interactions in the material surrounding the cryostat. The simulated events from both samples are then combined with events from an unbiased EXT sample (which is not filtered based on PMT activity) in order to simulate MicroBooNE's cosmic ray background [15]. Furthermore, MicroBooNE utilizes another sample of simulated events generated using the NuWro neutrino event generator [16] for additional studies.

The physics in both the Overlay MC and Dirt MC samples is given by the GENIE MicroBooNE Tune, a version of the GENIE v3.0.6 G18_10a_02_11a model set in which four parame-

ters are tuned to $\nu_\mu$ CC0$\pi$ data from the T2K experiment [17]. The four parameters are: the CC quasi-elastic axial mass [18], the strength of the random phase approximation (RPA) corrections in the Nieves CCQE cross section calculation [19], the absolute normalization of the CC2p2h cross section [20], the shape of the CC2p2h cross-section. The shape of the CC2p2h cross section is represented by a parameter that linearly interpolates between two models: the Valencia prediction [20] and the Dytman model [21].

## 3. Event Selection

The signal consists of charged-current muon-neutrino interactions within the fiducial volume with the final state particles consisting of exactly one muon with momentum $0.1 \leq \mathrm{P}_\mu \leq 1.2\,\mathrm{GeV}/c$ and two protons with momentum $0.3 \leq \mathrm{P}_p \leq 1.0\,\mathrm{GeV}/c$. Events with any number of neutral pions are excluded. Signal events may also contain protons with momentum below $0.3\,\mathrm{GeV}/c$ or above $1.2\,\mathrm{GeV}/c$, any number of neutrons and charged pions with momentum below $65\,\mathrm{MeV}/c$.

The BNB data, EXT data, overlay MC, and dirt MC samples are processed by the Pandora reconstruction framework [22] to identify and reconstruct tracks from the ionized signal. The track's energy deposition and length are used to reconstruct momentum and particle identification. From the reconstructed products, a series of selection requirements are applied to identify CC1$\mu$2p0$\pi$ events. The initial selection retains events that meet three criteria: (1) the reconstructed neutrino vertex is located within a fiducial volume (FV) defined to be at least 10 cm inside any TPC face, (2) there are exactly three tracks, and no showers as determined by Pandora [23], (3) the three tracks start within 4 cm of the reconstructed neutrino vertex. Particle identification techniques described in Ref. [24] are then used to identify events with a single muon candidate and two proton candidates.

The final event selection requires one muon with momentum in the range $0.1 \leq \mathrm{P}_\mu \leq 1.2\,\mathrm{GeV}/c$ and two protons, both with momentum in the range $0.3 \leq \mathrm{P}_p \leq 1.0\,\mathrm{GeV}/c$. The limits on momentum are driven by the resolution effects as well as phase space regions which have non-zero efficiencies and well understood systematic uncertainties. To benchmark the performance of the selection, the number of simulated CC1$\mu$2p0$\pi$ events that pass all selection requirements is compared to the number of events generated using the GENIE MicroBooNE tune; the event selection described above achieves an efficiency and purity of $\simeq$ 14% and $\simeq$ 65%, respectively. More details of the event selection can be found in Ref. [25].

In addition to studying theoretical predictions of 2p2h processes using the GENIE MicroBooNE Tune, we consider predictions from three additional GENIE model sets [18]: GENIE v3.0.6 G18_02a_00_000 (GENIE Empirical), GENIE v3.0.6 G18_10a_02_11a (GENIE Nieves), and GENIE v3.2.0 G21_11b_00_000 (GENIE SuSAv2). All three model sets utilize the same models for CC coherent pion production (CCCOH) [26], CC resonant pion production (CCRES), which is based on the Rein-Sehgal prediction, but uses updated form factors [27] and includes lepton mass effects and additional pion production diagrams [28, 29, 30], and CC deep inelastic scattering (CCDIS) [31, 32]. Further, the GENIE Empirical and GENIE Nieves model sets both utilize the hA2018 FSI model [33], while the GENIE SuSAv2 model set utilizes the hN2018 FSI model [34]. Note that the GENIE MicroBooNE Tune is identical to the GENIE Nieves model except for the four tuned parameters mentioned previously.

In addition to the two different FSI models, each GENIE model set uses distinct models for QE and MEC neutrino interaction modes. These distinctions in QE, MEC, and FSI models are critical as these components all have an impact on 2p2h processes. The GENIE Empirical model set uses the relativistic Fermi gas (RFG) nuclear model [35], the Llewellyn Smith QE model [36],

and an empirically derived prediction for MEC interactions [21]. The GENIE Nieves model set uses the local Fermi gas (LFG) nuclear model [37], which is similar to the RFG model but includes considerations for the nuclear density. The Nieves QE [38] model is similar to the Llewellyn Smith QE model, but includes contributions from long range nucleon-nucleon correlations and Coulombic effects. The Nieves MEC model is based on a macroscopic calculation [20]. The original SuSAv2 model set utilizes the relativistic mean field (RMF) approximation nuclear model [39, 40], which considers relativistic effects in the calculation of the motion of the nucleons in the nucleus. Relativistic effects are also considered in the calculation of the SuSAv2 QE [41] and SuSAv2 MEC [42] predictions by using scaling functions, derived from relativistic assumptions, to scale the cross sections at high momentum transfers. Although GENIE lacks the option to use an RMF nuclear model directly, it achieves approximate consistency with the RMF-based results by choosing the nucleon initial momentum from an LFG distribution. In addition, the default nucleon binding energy used in GENIE for the LFG model is replaced for SuSAv2 with an effective value tuned to most closely duplicate the RMF distribution [10, 43].

Beyond the GENIE generator predictions, the GiBUU 2023 [44], NuWro 19.02 [45], and NEUT 5.4.0 [46] model sets are also considered. The GiBUU model set uses similar models to GENIE, but they are consistently implemented to solve the Boltzmann-Uehling-Uhlenbeck transport equation [47]. It is based on an LFG model [48], using a standard CCQE expression [49] and an empirical MEC model. A spin-dependent resonance amplitude calculation is performed following [47]. The FSI treatment transports the hadrons through the residual nucleus in a potential consistent with the initial state. The NuWro model set is built on the same LFG model [48], using the Llewellyn Smith QE model [36], the Adler-Rarita-Schwinger [50] formalism to calculate the $\Delta$ resonance, and the Berger Sehgal CCCOH [26] scattering model. The FSI treatment uses an intranuclear cascade [51] to transport the hadrons through the nucleus, along with a coupling to `PYTHIA` for hadronization [52]. The NEUT model set utilizes an LFG model [48], with Nieves CCQE [38] and MEC [20] scattering model, the Berger Sehgal RES [28] and CCCOH [26] prescriptions and treats FSI with medium corrections for pions [14].

Using samples of simulated $\nu_\mu$ CC interactions from each model set, a study was conducted to identify variables sensitive to physics differences between the model sets. One such variable is the opening angle between the protons in the lab frame, $\theta_{\vec{P}_L \cdot \vec{P}_R}$, defined as:

$$\cos(\theta_{\vec{P}_L \cdot \vec{P}_R}) = \frac{\vec{P}_L \cdot \vec{P}_R}{\left|\vec{P}_L\right| \left|\vec{P}_R\right|} \tag{1}$$

where $\vec{P}_L$ is the momentum of the leading proton, the proton with the highest momentum, and $\vec{P}_R$ is the momentum of the recoil proton, the second proton in the event. A second physics-sensitive variable is the opening angle between the muon and total proton momentum vector, $\theta_{\vec{P}_\mu \cdot \vec{P}_{\text{sum}}}$, defined as:

$$\cos(\theta_{\vec{P}_\mu \cdot \vec{P}_{\text{sum}}}) = \frac{\vec{P}_\mu \cdot \vec{P}_{\text{sum}}}{\left|\vec{P}_\mu\right| \left|\vec{P}_{\text{sum}}\right|} \tag{2}$$

where $\vec{P}_\mu$ is the momentum of the muon and $\vec{P}_{\text{sum}}$ is the vector addition of the leading and recoil proton momenta. The opening angle between the protons in the lab frame provides information on the effect of the QE and MEC modeling on the proton momentum, while the opening angle between the muon and total proton momentum vectors provides information on the treatment of the outgoing muon momentum in relation to the 2p2h system.

In addition to these two angles, we also identify the magnitude of the momentum transverse to the neutrino beam direction of the final state system, $\delta P_T$ [53]. The transverse momentum vector of the CC1$\mu$2p0$\pi$ system ($\delta\vec{P}_T$) is defined as:

$$\delta\vec{P}_T = \vec{P}_T^{\mu} + \vec{P}_T^{L} + \vec{P}_T^{R} \tag{3}$$

where $\vec{P}_T^{\mu}$, $\vec{P}_T^{L}$, and $\vec{P}_T^{R}$ are the transverse momentum vectors of the muon, leading proton, and recoil proton respectively. The magnitude $\delta P_T$ is sensitive to nuclear effects, final state interactions, or below threshold undetected particles.

Distributions of selected events as a function of the cosine of $\theta_{\vec{P}_L\cdot\vec{P}_R}$ can be found in Fig. 1. The colored bands in each histogram represent events selected from the overlay MC subdivided into different final state topologies (Fig. 1(a)) and different interaction modes based on the GENIE MicroBooNE Tune prediction [Fig. 1(b)]. The error bars on the data points are the data statistical uncertainty while the dashed lines represent the uncertainty on the combination of the Overlay MC, Dirt MC, and EXT data (also known as the prediction). This uncertainty includes both the statistical uncertainty of the prediction and systematic uncertainty, which dominates over the data statistical uncertainty for this measurement. Contributions from flux modeling and protons-on-target (POT) counting [54], cross section modeling [17], re-interaction modeling [55], and detector modeling [56] are considered in the calculation of the systematic uncertainties, which was performed using the multiverse techniques described in Section V of Ref. [17]. Uncertainty on the modeling of dirt events is also considered in the systematic uncertainty [57]. We find that our CC1$\mu$2p0$\pi$ signal, represented by the blue-green bands in Fig. 1(a), constitutes the majority of events selected from the overlay MC sample. We also find that the CCMEC process, represented by the blue-green band in Fig. 1(b), has fewer events in the region of $\cos(\theta_{\vec{P}_L\cdot\vec{P}_R}) \simeq 0$ compared to the signal. This is expected as MEC is not the only contributor to CC1$\mu$2p0$\pi$ topologies. The comparison of the data points to the prediction shows reasonable shape agreement as well as normalization agreement.

## 4. Cross Section Extraction

Due to detector resolution, efficiency, and smearing effects, our reconstructed kinematic variables require unfolding. We use the Wiener-SVD technique [58] as implemented in [59]. In this technique, any bias due to regularization introduced by the unfolding is encoded in a regularization matrix $A_C$. To compare a theoretical prediction to the measurements, the prediction should first be multiplied by $A_C$; this transforms the prediction into the "regularized space" of the data so that a proper comparison can be made. Unfolded distributions are then normalized by the number of target nuclei and the total integrated neutrino flux to produce a cross section. We validate the Wiener-SVD unfolding technique by performing fake data studies before unfolding the selected BNB data events.

Fig. 2 shows the single differential cross sections as functions of cosine of $\theta_{\vec{P}_L\cdot\vec{P}_R}$ [Fig. 2(a)] and cosine of $\theta_{\vec{P}_\mu\cdot\vec{P}_{\text{sum}}}$ [Fig. 2(b)]. The black points represent the extracted cross section from data with the inner error bands representing the statistical uncertainty and the outer error bands representing the systematic uncertainty. Although MEC modeling uncertainties enter predominantly only through the efficiency, they are still the dominant cross-section uncertainties in some bins due to the large uncertainties assigned to this model which is itself due to the lack of previous measurements.

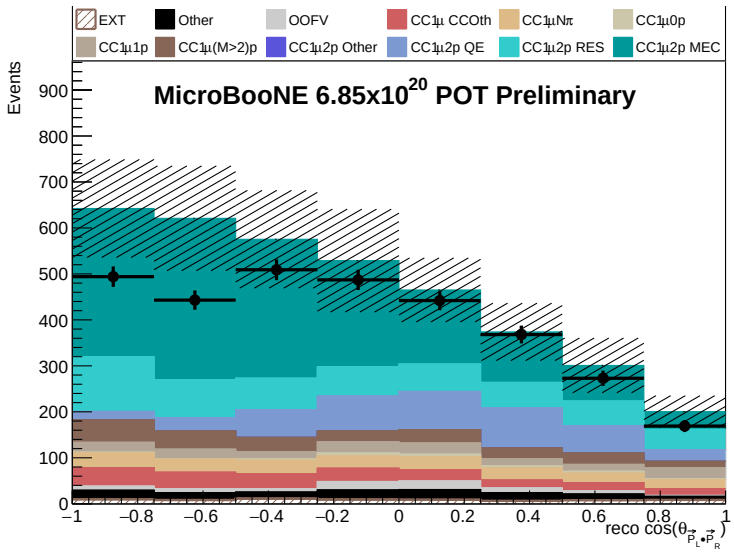


(a)

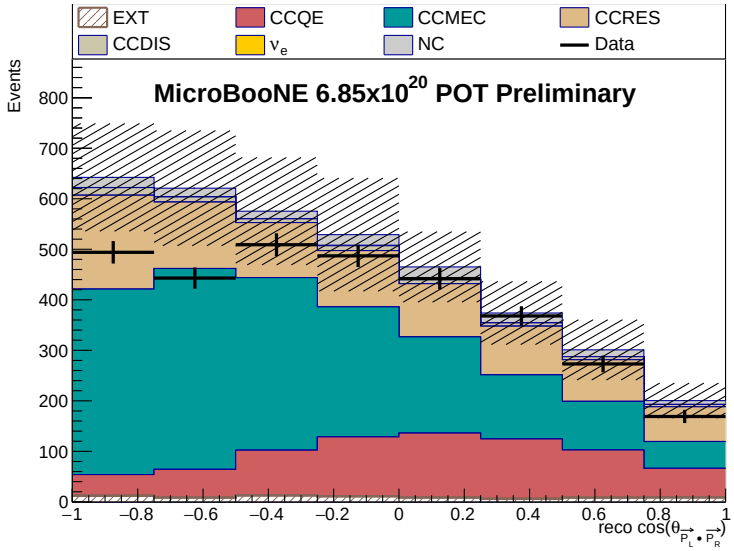


(b)

Figure 1: Yield for the cosine of the opening angle between the protons in the lab frame, $\theta_{\vec{P}_L \cdot \vec{P}_R}$. The selected MC events are broken down into (a) final-state topologies and (b) $\nu$ interaction channels based on the MicroBooNE Tune [17] truth information. The error on the data represents the data statistical uncertainty and the hatched region represents the statistical plus systematic uncertainty on the prediction.

When extracting the cross section from data, we find that the GiBUU, GENIE MicroBooNE Tune, and GENIE Nieves models have the best agreement with our data in $\cos(\theta_{\vec{P}_L \cdot \vec{P}_R})$, and the GiBUU and NEUT models have the best agreement with our data in $\cos(\theta_{\vec{P}_\mu \cdot \vec{P}_{\text{sum}}})$. The $\chi^2$ per

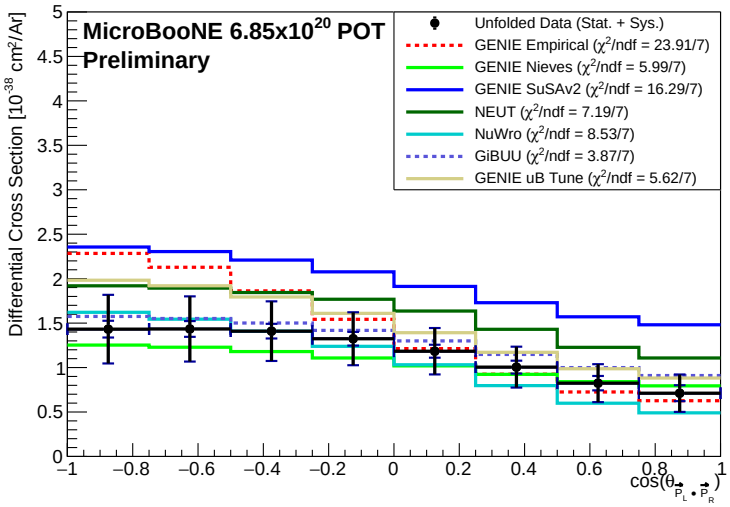


(a)

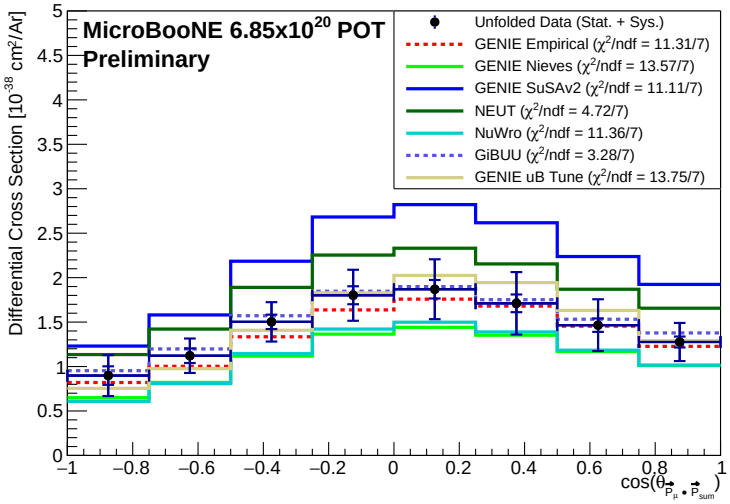


(b)

Figure 2: Single differential cross sections as a function of (a) the cosine of the opening angle between the protons in the lab frame, $\cos(\theta_{\vec{P}_L \cdot \vec{P}_R})$, and (b) the cosine of the opening angle between the muon and total proton momentum vector, $\cos(\theta_{\vec{P}_\mu \cdot \vec{P}_{\text{sum}}})$. The inner error bands on the data represent the statistical uncertainty while the outer error bands represent the systematic uncertainty. A $\chi^2$/ndf, considering systematic and statistical uncertainties, is calculated between the data and each model set curve. Details of the generator predictions are given in section 3.

degree of freedom ($\chi^2$/dof) is calculated between the data and each model set curve. The number of degrees of freedom is equal to the number of histogram bins minus one. Both systematic

and statistical uncertainties on the data are considered in this calculation. The GENIE MicroBooNE Tune and GENIE Empirical models tend to predict higher cross sections than indicated by our data in regions of low $\cos(\theta_{\vec{P}_L \cdot \vec{P}_R})$ and high $\cos(\theta_{\vec{P}_\mu \cdot \vec{P}_{\text{sum}}})$. Although the GENIE MicroBooNE Tune uses all the same model elements as the GENIE Nieves sample, we find an overall difference in shape and normalization between these two curves. This is most likely caused by the increased CC2p2h cross section normalization and interpolated CC2p2h cross section shape that are utilized in the GENIE MicroBooNE Tune. Additionally, the GENIE SuSAv2 model is overpredicted in both distributions which is likely caused by the increased CC2p2h cross section normalization.

We further show the single differential cross sections for the data and the models as functions of $\delta P_T$ in Fig. 3. In this variable, the NuWro prediction is higher than the data and other models in the first bin. The reason for this is that Nieves and NuWro form their initial hadronic states in different ways. In the GENIE implementation of the GENIE Nieves model set, two nucleons are selected from the Fermi sea of the nucleus [21]. The momentum of each nucleon is then randomly sampled from a distribution of the initial state nucleon momentum [20] formed from the LFG nuclear model [37]. In NuWro, the selection of the two nucleons and their momenta is similar to the GENIE implementation of GENIE Nieves, but the two nucleons are required to have back-to-back momenta in the initial state [60]. The over-prediction of NuWro at low $\delta P_T$ has also been observed in Ref. [61], which also finds this over-prediction in the absence of FSI, indicating that the excess is an initial state effect. Our data indicates that there is a preference for the NEUT and GiBUU model descriptions.

## 5. Conclusion

In this letter, we present the first measurement of single differential cross sections of CC1$\mu$2p0$\pi$ events on argon. Events containing exactly one muon, two protons, and no other mesons are selected from BNB data. We extract differential cross sections as functions of three kinematic variables, $\cos(\theta_{\vec{P}_L \cdot \vec{P}_R})$, $\cos(\theta_{\vec{P}_\mu \cdot \vec{P}_{\text{sum}}})$ and $\delta P_T$, which are found to be sensitive to the formation of 2p2h pairs through MEC processes. We compare our extracted cross sections to those predicted by the GENIE, GiBUU, NEUT, and NuWro generators, including four different GENIE model sets. These cross-section models span a range of nuclear models, QE and MEC models, and hadron transport models. We find that the GiBUU prediction shows the best overall shape agreement in the kinematic variables describing opening angles. The $\delta P_T$ variable is sensitive to the different initial hadronic states, and we find that NEUT gives the best overall description of the production of CC1$\mu$2p0$\pi$ final states. This is the first differential cross-section measurement of two-proton final states, and therefore the first time that these models can be directly compared to data. This provides valuable input for future model development toward precision neutrino physics measurements. In addition, these measured CC1$\mu$2p0$\pi$ cross sections can be used to reinterpret data from existing experiments that cannot distinguish 2p2h final states from other CC interaction mechanisms.

This document was prepared by the MicroBooNE collaboration using the resources of the Fermi National Accelerator Laboratory (Fermilab), a U.S. Department of Energy, Office of Science, HEP User Facility. Fermilab is managed by Fermi Research Alliance, LLC (FRA), acting under Contract No. DE-AC02-07CH11359. MicroBooNE is supported by the following: the U.S. Department of Energy, Office of Science, Offices of High Energy Physics and Nuclear Physics; the U.S. National Science Foundation; the Swiss National Science Foundation; the

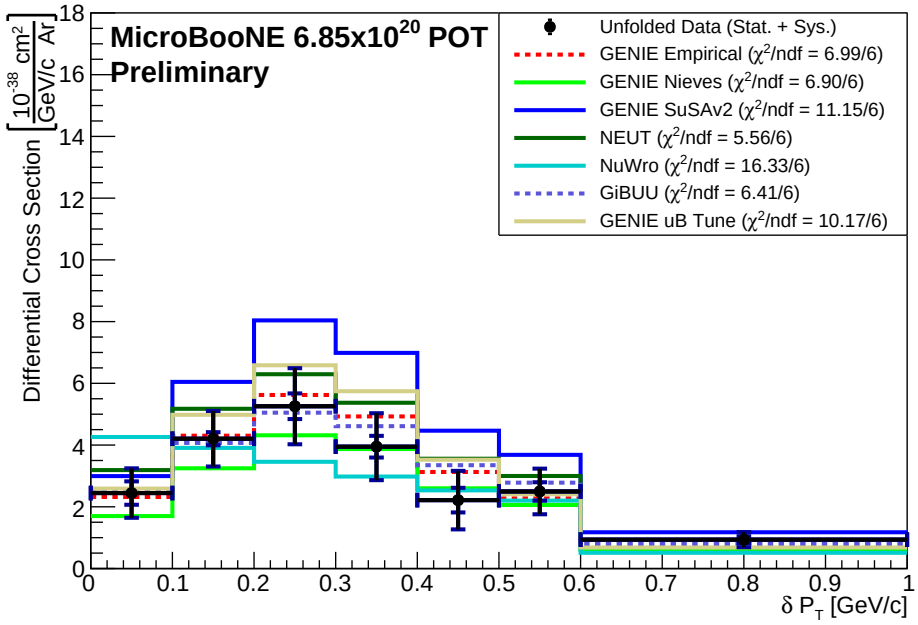


Figure 3: Single differential cross section as a function of the magnitude of the transverse momentum of the final state system, $\delta P_T = \left|\vec{P}_T^{\,\mu} + \vec{P}_T^{\,L} + \vec{P}_T^{\,R}\right|$. The inner error bands on the data represent the statistical uncertainty while the outer error bands represent the systematic uncertainty. A $\chi^2$/ndf, considering systematic and statistical uncertainties, is calculated between the data and each model set curve. Details of the generator predictions are given in section 3.

Science and Technology Facilities Council (STFC), part of the United Kingdom Research and Innovation; the Royal Society (United Kingdom); and the UK Research and Innovation (UKRI) Future Leaders Fellowship. Additional support for the laser calibration system and cosmic ray tagger was provided by the Albert Einstein Center for Fundamental Physics, Bern, Switzerland. We also acknowledge the contributions of technical and scientific staff to the design, construction, and operation of the MicroBooNE detector as well as the contributions of past collaborators to the development of MicroBooNE analyses, without whom this work would not have been possible. For the purpose of open access, the authors have applied a Creative Commons Attribution (CC BY) public copyright license to any Author Accepted Manuscript version arising from this submission.

## References

[1] C. Rubbia. The Liquid Argon Time Projection Chamber: A New Concept for Neutrino Detectors. *Reports No. CERN-EP-INT-77-08*, CERN-EP-77-08, 5 1977. URL ,http://cds.cern.ch/record/117852/.

[2] H. H. Chen, P. E. Condon, B. C. Barish, and F. J. Sciulli. A Neutrino Detector Sensitive to Rare Processes. I. A Study of Neutrino Electron Reactions. *FNAL Proposal 496*, 5 1976. URL https://inspirehep.net/files/df1edf05d33a55edbb411bdebb802f58.

[3] W.J. Willis and V. Radeka. Liquid-argon ionization chambers as total-absorption detectors. *Nucl. Instrum. Methods*, 120(2):221–236, 1974. ISSN 0029-554X. doi: https://doi.org/10.1016/0029-554X(74)90039-1. URL https://www.sciencedirect.com/science/article/pii/0029554X74900391.

[4] D. R. Nygren. The Time Projection Chamber: A New $4\pi$ Detector for Charged Particles. *eConf*, C740805:58, 1974. URL https://lss.fnal.gov/conf/C740805/p58.pdf.

[5] J. A. Formaggio and G. P. Zeller. From eV to EeV: Neutrino cross sections across energy scales. *Rev. Mod. Phys.*, 84:1307–1341, Sep 2012. doi: 10.1103/RevModPhys.84.1307. URL https://link.aps.org/doi/10.1103/RevModPhys.84.1307.

[6] L. Alvarez-Ruso and other. Neutrino scattering theory experiment collaboration white paper: Status and challenges of neutrino–nucleus scattering. *Progress in Particle and Nuclear Physics*, 100:1–68, 2018. ISSN 0146-6410. doi: https://doi.org/10.1016/j.ppnp.2018.01.006. URL https://www.sciencedirect.com/science/article/pii/S0146641018300061.

[7] Or Hen, Gerald A. Miller, Eli Piasetzky, and Lawrence B. Weinstein. Nucleon-nucleon correlations, short-lived excitations, and the quarks within. *Rev. Mod. Phys.*, 89:045002, Nov 2017. doi: 10.1103/RevModPhys.89.045002. URL https://link.aps.org/doi/10.1103/RevModPhys.89.045002.

[8] R. Cruz-Torres et al. Many-body factorization and position–momentum equivalence of nuclear short-range correlations. *Nature Phys.*, 17(3):306–310, 2021. doi: 10.1038/s41567-020-01053-7.

[9] I. Ruiz Simo, J.E. Amaro, M.B. Barbaro, J.A. Caballero, G.D. Megias, and T.W. Donnelly. Two-nucleon emission in neutrino and electron scattering from nuclei: The modified convolution approximation. *Annals of Physics*, 388: 323–349, 2018. ISSN 0003-4916. doi: https://doi.org/10.1016/j.aop.2017.11.029. URL https://www.sciencedirect.com/science/article/pii/S0003491617303512.

[10] S. Dolan, G. D. Megias, and S. Bolognesi. Implementation of the SuSAv2-meson exchange current 1p1h and 2p2h models in GENIE and analysis of nuclear effects in T2K measurements. *Phys. Rev. D*, 101:033003, Feb 2020. doi: 10.1103/PhysRevD.101.033003. URL https://link.aps.org/doi/10.1103/PhysRevD.101.033003.

[11] R. Acciarri et al. Detection of back-to-back proton pairs in charged-current neutrino interactions with the ArgoNeuT detector in the NuMI low energy beam line. *Phys. Rev. D*, 90:012008, Jul 2014. doi: 10.1103/PhysRevD.90.012008. URL https://link.aps.org/doi/10.1103/PhysRevD.90.012008.

[12] R. et al. Acciarri. Design and construction of the microboone detector. *Journal of Instrumentation*, 12(02): P02017–P02017, February 2017. ISSN 1748-0221. doi: 10.1088/1748-0221/12/02/p02017. URL http://dx.doi.org/10.1088/1748-0221/12/02/P02017.

[13] A. A. Aguilar-Arevalo et al. Neutrino flux prediction at MiniBooNE. *Phys. Rev. D*, 79:072002, Apr 2009. doi: 10.1103/PhysRevD.79.072002. URL https://link.aps.org/doi/10.1103/PhysRevD.79.072002.

[14] C. Andreopoulos et al. The GENIE Neutrino Monte Carlo Generator. *Nucl. Instrum. Meth. A*, 614:87–104, 2010. doi: 10.1016/j.nima.2009.12.009.

[15] C. Adams et al. Rejecting cosmic background for exclusive charged current quasi elastic neutrino interaction studies with Liquid Argon TPCs; a case study with the MicroBooNE detector. *Eur. Phys. J. C*, 79(8):673, 2019. doi: 10.1140/epjc/s10052-019-7184-7.

[16] T. Golan, J. T. Sobczyk, and J. Zmuda. NuWro: The Wroclaw Monte Carlo Generator of Neutrino Interactions. *Nucl. Phys. B Proc. Suppl.*, 229-232:499–499, 2012. doi: 10.1016/j.nuclphysbps.2012.09.136.

[17] P. Abratenko et al. New CC0$\pi$ GENIE model tune for MicroBooNE. *Phys. Rev. D*, 105(7):072001, 2022. doi: 10.1103/PhysRevD.105.072001.

[18] Luis Alvarez-Ruso et al. Recent highlights from GENIE v3. *Eur. Phys. J. ST*, 230(24):4449–4467, 2021. doi: 10.1140/epjs/s11734-021-00295-7.

[19] J. Nieves, J. E. Amaro, and M. Valverde. Inclusive quasielastic charged-current neutrino-nucleus reactions. *Phys. Rev. C*, 70:055503, Nov 2004. doi: 10.1103/PhysRevC.70.055503. URL https://link.aps.org/doi/10.1103/PhysRevC.70.055503.

[20] Jackie Schwehr, Dan Cherdack, and Rik Gran. Genie implementation of ific valencia model for qe-like 2p2h neutrino-nucleus cross section. 2016. URL https://doi.org/10.48550/arXiv.1601.02038.

[21] Teppei Katori. Meson Exchange Current (MEC) Models in Neutrino Interaction Generators. *AIP Conf. Proc.*, 1663 (1):030001, 2015. doi: 10.1063/1.4919465.

[22] R. Acciarri et al. The Pandora multi-algorithm approach to automated pattern recognition of cosmic-ray muon and neutrino events in the MicroBooNE detector. *Eur. Phys. J. C*, 78(1):82, 2018. doi: 10.1140/epjc/s10052-017-5481-6.

[23] Wouter Van De Pontseele. Search for Electron Neutrino Anomalies with the MicroBooNE Detector. PhD thesis, Oxford U., 2020.

[24] P. Abratenko et al. Calorimetric classification of track-like signatures in liquid argon TPCs using MicroBooNE data. *J. High Energy Phys.*, 12:153, 2021. doi: 10.1007/J.HighEnergyPhys.12(2021)153.

[25] Samantha Sword-Fehlberg. First Measurement Of Charged-Current 1 Muon 2 Proton 0 Pion Single Differential Cross-Sections on Argon-40 at 0.8 GeV Average Neutrino Energy with The MicroBooNE Detector. PhD thesis, New Mexico State U., 2022. URL https://inspirehep.net/files/86513c78e44015c4f1bdd4b070daca9f.

[26] Ch. Berger and L. M. Sehgal. PCAC and coherent pion production by low energy neutrinos. *Phys. Rev. D*, 79: 053003, 2009. doi: 10.1103/PhysRevD.79.053003.

[27] Krzysztof M. Graczyk and Jan T. Sobczyk. Lepton mass effects in weak charged current single pion production. *Phys. Rev. D*, 77:053003, Mar 2008. doi: 10.1103/PhysRevD.77.053003. URL https://link.aps.org/doi/10.1103/PhysRevD.77.053003.

[28] Ch. Berger and L. M. Sehgal. Lepton mass effects in single pion production by neutrinos. *Phys. Rev. D*, 76:113004, Dec 2007. doi: 10.1103/PhysRevD.76.113004. URL https://link.aps.org/doi/10.1103/PhysRevD.76.113004.

[29] Konstantin S. Kuzmin, Vladimir V. Lyubushkin, and Vadim A. Naumov. Lepton polarization in neutrino nucleon interactions. *Mod. Phys. Lett. A*, 19:2815–2829, 2004. doi: 10.1142/S0217732304016172.

[30] Jaroslaw A. Nowak. Four Momentum Transfer Discrepancy in the Charged Current $\pi^+$ Production in the MiniBooNE: Data vs. Theory. *AIP Conf. Proc.*, 1189(1):243–248, 2009. doi: 10.1063/1.3274164.

[31] U. K. Yang and A. Bodek. Studies of higher twist and higher order effects in NLO and NNLO QCD analysis of lepton nucleon scattering data on $F_2$ and $R = \sigma_L/\sigma_T$. *Eur. Phys. J. C*, 13:241–245, 2000. doi: 10.1007/s100520000320.

[32] A Bodek and U. K. Yang. Higher twist, $\xi(\omega)$ scaling, and effective LO PDFs for lepton scattering in the few GeV region. *J. Phys. G*, 29:1899–1906, 2003. doi: 10.1088/0954-3899/29/8/369.

[33] D. Ashery et al. True absorption and scattering of pions on nuclei. *Phys. Rev. C*, 23:2173–2185, May 1981. doi: 10.1103/PhysRevC.23.2173. URL https://link.aps.org/doi/10.1103/PhysRevC.23.2173.

[34] L. A. Harewood and R. Gran. Elastic hadron-nucleus scattering in neutrino-nucleus reactions and transverse kinematics measurements. 6 2019. URL https://doi.org/10.48550/arXiv.1906.10576.

[35] R. A. Smith and E. J. Moniz. Neutrino reactions on nuclear targets. *Nucl. Phys. B*, 43:605, 1972. doi: 10.1016/0550-3213(75)90612-4. [Erratum: Nucl.Phys.B 101, 547 (1975)].

[36] C. H. Llewellyn Smith. Neutrino Reactions at Accelerator Energies. *Phys. Rept.*, 3:261–379, 1972. doi: 10.1016/0370-1573(72)90010-5.

[37] J. Nieves, J. E. Amaro, and M. Valverde. Inclusive quasielastic charged-current neutrino-nucleus reactions. *Phys. Rev. C*, 70:055503, Nov 2004. doi: 10.1103/PhysRevC.70.055503. URL https://link.aps.org/doi/10.1103/PhysRevC.70.055503.

[38] J. Nieves, F. Sanchez, I. Ruiz Simo, and M. J. Vicente Vacas. Neutrino Energy Reconstruction and the Shape of the CCQE-like Total Cross Section. *Phys. Rev. D*, 85:113008, 2012. doi: 10.1103/PhysRevD.85.113008.

[39] Brian D. Serot and John Dirk Walecka. *Relativistic Nuclear Many-Body Theory*, pages 49–92. Springer US, Boston, MA, 1992. ISBN 978-1-4615-3466-2. doi: 10.1007/978-1-4615-3466-2_5. URL https://doi.org/10.1007/978-1-4615-3466-2_5.

[40] J. A. Caballero, J. E. Amaro, M. B. Barbaro, T. W. Donnelly, C. Maieron, and J. M. Udias. Superscaling in charged current neutrino quasielastic scattering in the relativistic impulse approximation. *Phys. Rev. Lett.*, 95:252502, Dec 2005. doi: 10.1103/PhysRevLett.95.252502. URL https://link.aps.org/doi/10.1103/PhysRevLett.95.252502.

[41] S. Dolan, G. D. Megias, and S. Bolognesi. Implementation of the SuSAv2-meson exchange current 1p1h and 2p2h models in GENIE and analysis of nuclear effects in T2K measurements. *Phys. Rev. D*, 101:033003, Feb 2020. doi: 10.1103/PhysRevD.101.033003. URL https://link.aps.org/doi/10.1103/PhysRevD.101.033003.

[42] T. W. Donnelly and Ingo Sick. Superscaling in inclusive electron - nucleus scattering. *Phys. Rev. Lett.*, 82:3212–3215, 1999. doi: 10.1103/PhysRevLett.82.3212.

[43] A. Papadopoulou et al. Inclusive electron scattering and the genie neutrino event generator. *Phys. Rev. D*, 103:113003, Jun 2021. doi: 10.1103/PhysRevD.103.113003. URL https://link.aps.org/doi/10.1103/PhysRevD.103.113003.

[44] U. Mosel and K. Gallmeister. Lepton-induced reactions on nuclei in a wide kinematical regime. *Physical Review D*, 109(3), February 2024. ISSN 2470-0029. doi: 10.1103/physrevd.109.033008. URL http://dx.doi.org/10.1103/PhysRevD.109.033008.

[45] T. Golan, J.T. Sobczyk, and J. Żmuda. Nuwro: the wrocław monte carlo generator of neutrino interactions. *Nuclear Physics B - Proceedings Supplements*, 229–232:499, August 2012. ISSN 0920-5632. doi: 10.1016/j.nuclphysbps.2012.09.136. URL http://dx.doi.org/10.1016/j.nuclphysbps.2012.09.136.

[46] Yoshinari Hayato and Luke Pickering. The neut neutrino interaction simulation program library. *The European Physical Journal Special Topics*, 230(24):4469–4481, October 2021. ISSN 1951-6401. doi: 10.1140/epjs/s11734-021-00287-7. URL http://dx.doi.org/10.1140/epjs/s11734-021-00287-7.

[47] Ulrich Mosel. Neutrino event generators: foundation, status and future. *Journal of Physics G: Nuclear and Particle Physics*, 46(11):113001, September 2019. ISSN 1361-6471. doi: 10.1088/1361-6471/ab3830. URL http://dx.doi.org/10.1088/1361-6471/ab3830.

[48] R.C. Carrasco and E. Oset. Interaction of real photons with nuclei from 100 to 500 mev. *Nuclear Physics A*, 536(3–4):445–508, January 1992. ISSN 0375-9474. doi: 10.1016/0375-9474(92)90109-w. URL http://dx.doi.org/10.1016/0375-9474(92)90109-W.

[49] T. Leitner, L. Alvarez-Ruso, and U. Mosel. Charged current neutrino-nucleus interactions at intermediate energies. *Physical Review C*, 73(6), June 2006. ISSN 1089-490X. doi: 10.1103/physrevc.73.065502. URL http://dx.doi.org/10.1103/PhysRevC.73.065502.

[50] Krzysztof M. Graczyk and Jan T. Sobczyk. Form factors in the quark resonance model. *Physical Review D*, 77(5), March 2008. ISSN 1550-2368. doi: 10.1103/physrevd.77.053001. URL http://dx.doi.org/10.1103/PhysRevD.77.053001.

[51] J. Nieves, I. Ruiz Simo, and M. J. Vicente Vacas. Inclusive charged-current neutrino-nucleus reactions. *Physical Review C*, 83(4), April 2011. ISSN 1089-490X. doi: 10.1103/physrevc.83.045501. URL http://dx.doi.org/10.1103/PhysRevC.83.045501.

[52] Torbjörn Sjöstrand, Stephen Mrenna, and Peter Skands. Pythia 6.4 physics and manual. *Journal of High Energy Physics*, 2006(05):026–026, May 2006. ISSN 1029-8479. doi: 10.1088/1126-6708/2006/05/026. URL http://dx.doi.org/10.1088/1126-6708/2006/05/026.

[53] X. G. Lu et al. Measurement of nuclear effects in neutrino interactions with minimal dependence on neutrino energy. *Phys. Rev. C*, 94(1):015503, 2016. doi: 10.1103/PhysRevC.94.015503.

[54] A. A. Aguilar-Arevalo et al. First measurement of the muon antineutrino double-differential charged-current quasielastic cross section. *Phys. Rev. D*, 88(3):032001, 2013. doi: 10.1103/PhysRevD.88.032001.

[55] J. Calcutt, C. Thorpe, K. Mahn, and Laura Fields. Geant4Reweight: a framework for evaluating and propagating hadronic interaction uncertainties in Geant4. *J. Instrum.*, 16(08):P08042, 2021. doi: 10.1088/1748-0221/16/08/P08042.

[56] P. Abratenko et al. Novel approach for evaluating detector-related uncertainties in a LArTPC using MicroBooNE data. *Eur. Phys. J. C*, 82(5):454, 2022. doi: 10.1140/epjc/s10052-022-10270-8.

[57] P. Abratenko et al. Search for an anomalous excess of inclusive charged-current $\nu_e$ interactions in the MicroBooNE experiment using Wire-Cell reconstruction. *Phys. Rev. D*, 105(11):112005, 2022. doi: 10.1103/PhysRevD.105.112005.

[58] W. Tang, X. Li, X. Qian, H. Wei, and C. Zhang. Data Unfolding with Wiener-SVD Method. *JINST*, 12(10):P10002, 2017. doi: 10.1088/1748-0221/12/10/P10002.

[59] Steven Gardiner. Mathematical methods for neutrino cross-section extraction. *arXiv*, 1 2024. doi: 10.48550/arXiv.2401.04065. URL https://arxiv.org/abs/2401.04065.

[60] Kajetan Niewczas and Jan T. Sobczyk. Search for nucleon-nucleon correlations in neutrino-argon scattering. *Phys. Rev. C*, 93(3):035502, 2016. doi: 10.1103/PhysRevC.93.035502.

[61] Lars Bathe-Peters. Studies of Single-Transverse Kinematic Variables for Neutrino Interactions on Argon. Master's thesis, Berlin Tech U., Harvard U., 2020.